Energy 266 (2023) 126409

Contents lists available at ScienceDirect

Energy

journal homepage: www.elsevier.com/locate/energy

Effect of natural and forced charge air humidity on the performance and emissions of a compression-ignition engine operating at high warm altitude

José Ramón Serrano [a], Jaime Martín [a], Pedro Piqueras [a,*], Roberto Tabet [a], Javier Gómez [b]

[a] Universitat Politècnica de València, CMT-Motores Térmicos, Camino de Vera s/n, 46022 Valencia, Spain
[b] HORIBA Europe GmbH, Germany

ARTICLE INFO

Keywords:
Ambient humidity
Altitude
Compression-ignition engine
Performance
Pollutant emissions

ABSTRACT

The effect of ambient humidity on the performance and pollutant emissions of internal combustion engines is not considered in the literature despite type-approval criteria are moving closer to real driving conditions. This work analyses experimentally the effects of charge air humidity at high warm altitudes, where the use of exhaust gas recirculation (EGR) is typically lowered and even avoided to recover engine performance at the expense of NOx emissions increase, on the response of a compression-ignition engine under a wide range of steady-state conditions in terms of engine-out emissions and specific fuel consumption. The impact of specific humidity variations within the atmospheric range was analysed by coupling the engine to an altitude simulator with pressure, temperature, and humidity control capabilities. High altitudes and warm & high ambient temperatures were explored (2000 m at 30 °C and 2500 m at 45 °C) to cover ambient specific humidity up to 30 g_{water}/kg_{dry_air}. In addition, the effects of increasing the specific humidity above the atmospheric levels were considered at 2500 m and 45 °C to emulate forced injection of water in the engine intake line corresponding to 60 g_{water}/kg_{dry_air}. With this approach, understanding of the role of humidity is provided to highlight its importance as additional ambient property in emission control. In parallel, the assessment of the forced water content increase to control NOx emissions when EGR must be lowered was performed due to the altitude impact on the engine performance and turbocharger limits. The results showed a consistent and significant reduction in engine-out NOx emissions as the ambient humidity increased, reaching up to 300% with respect to the dry case, caused by the decrease in O_2 availability due to the water content increase. The benefits of high humidity in NOx emission control at high altitudes when EGR is not feasible were complemented by an improved trade-off with particulate matter emission compared to the standard from EGR use. The results evidenced a reduction in opacity close to 250% for a given engine-out NOx emission when EGR was replaced by water content. By contrast, the slowdown of the combustion process as the fresh air humidity increased deteriorated the specific fuel consumption significantly as the engine load and speed increased. Nevertheless, these penalties ranged from 2 to 2.7% in the worst conditions and showed the same sensitivity for EGR and humidity increases.

1. Introduction

The ambient humidity is one of the main factors that feature the boundary conditions automotive engines work. Despite it is not considered a boundary condition for type-approval procedures [1], it conditions the charge air flow properties in addition to ambient pressure and temperature [2]. Several studies regarding water injection, with the fuel or indirectly in the intake manifold, show adverse effects on the combustion efficiency as the water content increases. Literature has described the impact of water content on the engine performance and pollutant emissions in different types of engines, such as gas turbines [3], spark-ignition engines [4–6], and compression-ignition engines, for both medium-duty [7,8] and heavy-duty applications [9], with common trends in all this variety of applications. In reciprocating internal combustion engines, the water injection significantly affects the combustion process, delaying the combustion start and reducing the maximum heat released during the main combustion phase. The combustion slowdown leads to the reduction of the engine efficiency [10], which forces an increase in the amount of fuel injected to maintain the power output of the engine [11]. In turn, the subsequent higher equivalence ratio gives as a result the increase of the CO and PM emissions as the injection of water increases [12]. The THC emissions also increase [12], since the combustion delay and the additional fuel mass increase the unburned

* Corresponding author.
E-mail address: pedpicab@mot.upv.es (P. Piqueras).

https://doi.org/10.1016/j.energy.2022.126409
Received 5 May 2022; Received in revised form 3 November 2022; Accepted 10 December 2022
Available online 15 December 2022

Nomenclature

η_V	Volumetric efficiency
BMEP	Brake mean effective pressure
BSFC	Brake specific fuel consumption
CA	Crank angle
DOC	Oxidation catalyst
EGR	Exhaust gas recirculation
HP-EGR	High-pressure EGR
ICE	Internal Combustion Engine
LP-EGR	Low-pressure EGR
$\dot{m}$	Mass flow
MEDAS	Multifunctional Efficient and Dynamic Altitude Simulator
MHM	MEDAS Humidity Module
MTM	MEDAS Temperature Module
n	Engine speed
p	Pressure
PM	Particulate matter
R	Gas constant
RH	Relative Humidity
RoHR	Rate of Heat Release
SCRf	Selective catalytic reduction filter
t/t	Total variables at the inlet and outlet of the compressor
T	Temperature
v	Specific volume
V_D	Engine displacement
WCAC	Water charge air cooler
Y	Mass fraction

fuel during the post-injection phase, leaving the cylinder before being completely oxidised. However, NO_x generation is significantly reduced due to the lower amount of available O_2 during the main phase of the combustion [13]. As a result, water injection shows potential as an alternative way to control the NO_x emissions in a compression-ignition engine [14]. Hountalas et al. [9] reasoned that the delay of the main combustion and the increase in the fuel mass lead to a higher amount of unburned fuel when the post-injection combustion phase starts. Although it penalises the THC emissions, the particulate matter (PM) oxidation generated during the main combustion enhances.

Despite previous works related to water injection in the intake air path, up to the author's knowledge, there are not published studies regarding the effect of the ambient humidity at altitude and hot air conditions. However, these driving conditions correspond to the highest specific humidity levels. In addition, no published works study the effect of forcing humidity beyond these attainable atmospheric levels at high altitude and temperature. In this context, this paper aims to understand further the impact of the water content in the charge air in terms of engine performance and engine-out emissions. The focus is driven toward the specific humidity influence on the response of a turbocharged compression-ignition engine at high altitude and ambient temperature. Under these ambient boundaries, the exhaust gas recirculation rate tends to be lowered and even completely avoided to recover part of the engine performance deteriorated by the altitude [15], although at the expense of the NOx emission increase [16]. In addition, a negative impact on the soot generation also appears at high altitude [17,18]. In this study, the way the humidity impacts the engine response evidences the need to consider this parameter as an additional boundary in emission regulations. The ambient humidity variability monitoring and the use of forced water injection offer a relevant potential for an optimised NOx and PM control, especially when EGR use is not possible because of the ambient boundaries impact on the engine performance and turbocharger operational limits.

Several options are available to study the effect of the change in ambient humidity on an internal combustion engine (ICE) in a test bench. The most common alternatives are water atomisers, vapour generators, and airstream crossing bubbling water columns. The atomised water accurately controls the amount of water injected into the air stream. However, it needs a long piping length to provide enough time to complete the water droplets break up, vaporisation and mix with the air mass flow [19]. Vapour generators regulate the specific humidity through the amount of vapour mixed with the air stream. It is one of the most used solutions to simulate humidity ranges at room pressure of the air charge for powertrains, such as fuel cells or ICEs. However, the maximum amount of vapour is limited due to the high electrical power requirements of vapour generation. In addition, commercial systems do not withstand overpressure or vacuum due to technical and regulatory constraints for vapour generators, so their use is limited to room pressure conditions [20]. Both aspects restrict the possibility of obtaining high specific humidity found at high altitude driving [21], as it naturally happens in several places on Earth.

Lastly, the bubbling water column moistens the air up to 100% in relative humidity (RH). Therefore, the humidity control must be combined with by-pass valves for the air stream to reach the target humidity [22]. This solution allows a wide range of air charge humidity without needing boiling water or extra piping length. In this regard, the methodology applied in this work is based on using an atmosphere-simulator MEDAS, designed by the authors and currently commercialised by HORIBA. MEDAS is coupled with a temperature modifier (MTM) and a humidity modifier (MHM), the latter based on bubbling water columns [23,24]. This kind of experimental facility can reproduce specific atmospheric conditions at the intake and exhaust of an ICE [25], being possible to emulate any ambient condition found in real driving operation by controlling pressure, temperature and humidity separately. MEDAS + MTM + MHM was used to flexibly condition the air fed to the turbocharged compression-ignition engine into a wide range of ambient boundaries to identify the role of the fresh air humidity on the engine performance and emissions patterns. Moreover, this study has achieved relative humidity levels higher than those likely at any altitude and ambient condition, thus entering the analysis of forced water injection impact as a natural extension of ambient influence.

2. Experimental setup and methods

This experimental study was conducted in a Euro 6 compression-ignition engine. Its main characteristics are listed in Table 1. It was equipped with a variable geometry turbine (VGT) and water-air charger cooler (WCAC) for boost control, as well as high-pressure (HP) and low-pressure (LP) exhaust gas recirculation (EGR) controlling the engine-out NO_x emissions. LP-EGR was used in this study since the HP-EGR strategy only worked during engine warm-up phases. The aftertreatment system

Table 1
Specifications of the engine.

Type	Euro 6 compression-ignition engine
Displacement	1995 cm^3
Bore	84 mm
Stroke	90 mm
Number of cylinders	4 in line
Number of valves	4 per cylinder
Compression ratio	16.0:1
Maximum power @ speed	147 kW @ 3500 rpm
Maximum torque @ speed	400 Nm @ 1750 rpm
Maximum mass flow @ speed	630 kg/h @ 3500 rpm & full load
Boosting system	VGT and WCAC
EGR type	HP and cooled LP-EGR
Aftertreatment	Closed-coupled DOC + SCRf

comprised a close-coupled oxidation catalyst (DOC) and a wall-flow particulate filter coated as a selective catalytic reduction system (SCRf). However, the urea injection was omitted in this work so that the SCRf acted as a conventional wall-flow particulate filter.

The engine was coupled to an asynchronous dynamometer controlled by the AVL PUMA Open system to set engine torque and speed. An AVL GU21D glow-plug piezoelectric pressure transducer measured the instantaneous in-cylinder pressure. In addition, the engine intake and exhaust systems were instrumented with Wika piezoresistive pressure sensors and K-type thermocouples for pressure and temperature measurement. An AVL Flowsonix air mass flow sensor and an AVL 733S gravimetric balance monitored the air and fuel mass flows. Finally, the engine-out pollutants emissions were measured by a Horiba MEXA ONE gas analyser and an AVL 439 Opacimeter placed upstream of the aftertreatment system. In addition, a gas sample was also taken from the intake manifold to obtain the CO_2 molar fraction and calculate the EGR rate.

The intake air conditions supplied to the engine were governed by the altitude simulator Horiba MEDAS coupled to the engine. In particular, the altitude simulator was connected to MEDAS temperature (MTM) and humidity (MHM) modules for accurate control of pressure, temperature, and humidity of the supplied air in order to provide conditions at 2000 m and 30 °C and at 2500 m and 45 °C, respectively, depending on the test campaign. Fig. 1 shows the altitude simulator coupling to the engine intake, exhaust, and blow-by for complete conditioning of the engine systems to the working emulated ambient pressure. This kind of altitude simulator assembly has already been used in previous works. The concept and capabilities of MEDAS were presented in Ref. [21], while the altitude affects the pollutant emissions of a diesel engine were studied in Ref. [25]. The altitude and ambient temperature impact on calibration strategies for synergistic fuel consumption reduction and exhaust temperature increase for faster aftertreatment warm-up was also addressed in Ref. [16]. In fact, the use of MEDAS use enabled identifying, under controlled conditions, the effects of extreme altitude operation on the conversion efficiency of oxidation catalysts [26] and the regeneration capability of particulate filters [27]. Furthermore, Roberts et al. [28] used the atmospheric simulator set to reproduce the ambient conditions during on-road tests in an engine test bench with great accuracy.

The study analysed the dependence of the engine performance and emissions on the ambient humidity under steady-state operating conditions. A high altitude of 2000 m (0.797 bar) at 30 °C in ambient temperature was considered to cover the effects on the engine behaviour within a wide range of specific humidity. The engine response was mapped from 1500 to 3000 rpm in engine speed and from 4 to 15 bar in brake mean effective pressure (BMEP). This engine operation region was selected since it is where the maximum efficiency and torque are found and is representative in real driving conditions. In addition, it was also suitable to provide a common operating area for most of the parametric studies conducted to analyse the sensitivity to the specific humidity in the charge air flow and to the LP-EGR rate, as described next. In particular, every operating point was tested with three levels of LP-EGR rates, namely 0%, 5%, and 10%. The relative humidity was swept from 10 to 85% for each operating condition, with 40% and 70% as intermediate points. Therefore, the specific humidity of the fresh air mass flow ranged between 3 and 30 g_{water}/kg_{dry_air}. This last value corresponds to the maximum humidity registered on Earth in Mawsynram (India) [29], located at a high altitude with hot yearly averaged temperatures. The study was completed with a double-check campaign at an even higher altitude (2500 m) and ambient temperature (45 °C). These conditions were explicitly selected to analyse the engine response again at a medium-high specific humidity (10 and 30 g_{water}/kg_{dry_air}), enabling higher values without condensation. This way, the impact on the engine performance and emissions of operating with 60 g_{water}/kg_{dry_air} was finally measured. Although the last specific humidity is out of the atmosphere range, it adds a feature to the analysis by extrapolating the findings from the ambient boundaries to operation under forced water injection.

As a basis of the uncertainty analysis, Table 2 lists the uncertainty in percentage of the sensor span of the instrumentation used in this work. The uncertainty analysis of the direct measurements and derived quantities was performed by applying the methodology proposed by Olmeda et al. [30]. Several application examples can be found in Ref. [30]. In particular, the method is based on the fact that the

Table 2
Test cell instrumentation accuracy.

Instrument/sensor	Uncertainty [% of sensor span]
Dynamometer	0.018
Encoder	0.05
AVL GU21D Glow-plug piezoelectric pressure transducer	0.3
Wika Piezoresistive pressure sensor	0.5
K-Type thermocouple	0.75
AVL Flowsonix air mass flow meter	1
AVL 733S Gravimetric balance	0.12
Horiba MEXA ONE Gas analyser	1
AVL 439 Opacimeter	0.1

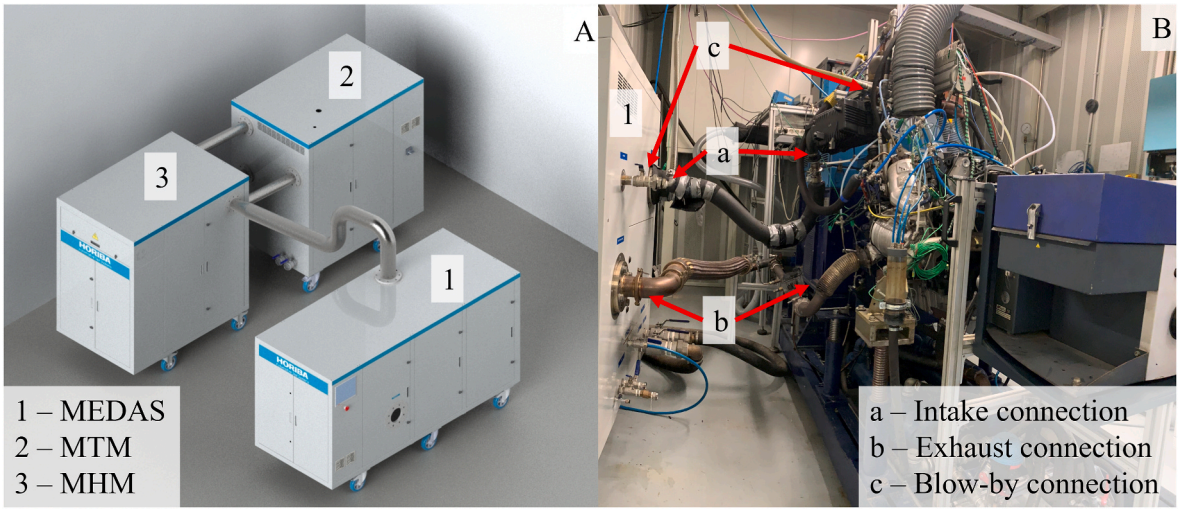

Fig. 1. MEDAS to engine connections. (A) MEDAS, MTM, and MHM layout; (B) MEDAS and engine coupling.

uncertainty in direct measurements is propagated to derived quantities that are of interest in the analysis of the engine response. For a given derived quantity z, its uncertainty u_z can be computed as

$$u_z^2 = \sum_i^n \left(\frac{\delta z}{\delta x_i}\right)^2 u_{x_i}^2 \quad (1)$$

where u_{x_i} is the uncertainty of the variable, and it is assumed that there is no correlation between the measurements. All figures except the contour maps show the uncertainty corresponding to each measurement. To complement the analysis of these maps, Table 3 compiles the maximum uncertainty found in the test campaign for each variable discussed in the paper. The resulting maximum uncertainties are highly below the differences found when analysing the impact of the specific humidity of the charge air flow and the EGR rate at every engine operating point and ambient driving conditions (altitude, ambient temperature).

3. Discussion of the results

3.1. Impact of humidity on fresh air charge and its O_2 content

For the sake of understanding, and taking Fig. 2A as an example, the EGR rate and the specific humidity are represented in the main-external x-axis and y-axis, respectively. The engine maps were measured for every EGR-humidity condition displayed. The relevant engine parameters are shown as a function of the engine speed in the secondary-internal x-axis and the engine load in the secondary-internal y-axis. Lastly, the measured points are identified by black dots in every contour. The results shown in Fig. 2A evidence that the fresh air mass flow decreased progressively as the specific humidity increased, in a similar way that the caused by the EGR rate increase. The central column (5% of LP-EGR) shows that the engine mapping was not completed when the humidity increased to 30 g_{water}/kg_{dry_air}. It was due to the opacity increase (Fig. 2B). Fig. 2B shows how the chart corresponding to 5% of LP-EGR rate and 13 g_{water}/kg_{air} in ambient specific humidity reached an opacity higher than 25% at 1500 rpm and 15 bar of BMEP. When the smoke limit was reached after increasing the specific humidity to 23 g_{water}/kg_{dry_air}, the ECU limited the injected fuel mass, failing to get the target BMEP (15 bar BMEP in this case). Fig. 2 shows how the maximum BMEP at 1500 rpm was further limited by excessive opacity when the LP-EGR rate was increased to 10%. These results highlight the relevant role of humidity on engine performance and drivability under real-drive conditions and limit the range of loads within the scope of interest for analysis.

Fig. 3 shows the fresh air mass flow when the altitude was increased to 2500 m and the ambient temperature set at 45 °C. As described in Section 2, the specific humidity of the fresh air charge was increased to 60 g_{water}/kg_{dry_air} to cover ambient and forced water injection levels. As expected, the fresh air mass flow decreased as the LP-EGR rate and the specific humidity increased, in agreement with the observed trend with natural moisture. The operating window affected by the smoke limiter was widened concerning conditions in Fig. 2B due to the higher altitude and ambient temperature. These two factors must be considered when comparing the sets of tests represented Figs. 2 and 3.

Table 3
Maximum uncertainty of the variables analysed in this study applying the methodology proposed by Olmeda et al. [30].

Variable	Units	Accuracy
BSFC	[g/kWh]	1.026
Fresh air mass flow	[kg/h]	0.816
O_2-to-fuel ratio	[−]	0.034
O_2	[%]	0.038
CO_2	[kg/h]	0.726
CO	[g/h]	1.693
THC	[g/h]	0.324
NO_X	[g/h]	5.931
Opacity	[%]	0.010
Soot	[g/h]	0.174

To confirm this general trend shown by both natural and forced conditions, Fig. 4A complements with the effect of reducing the fresh air mass flow on the engine-out oxygen molar fraction. Since each EGR and humidity set swept the same BMEP range, the exhaust gas O_2 reduction involves a higher equivalence ratio. Additionally, Fig. 4B shows the operation points plotted in the compressor map. The compressor operation moved gradually toward the surge line as the humidity increased, keeping the pressure ratio. The ambient pressure, the ambient temperature, and the boost pressure were imposed as boundary constants for each tested operating point. Therefore, the reasons for the decrease in the compressor mass flow (LP-EGR + fresh air) as the humidity increased were governed by two phenomena: the reduction of the density (due to gas constant increase) and the decrease of the volumetric efficiency [31]. The gas constant for the atmospheric air (R_{air}) and the volumetric efficiency (η_V) were calculated according to Eqs. (2) and (3).

R_i represents the gas constant for every air component, and Y_i accounts for the corresponding mass fraction. For example, at 2500 m and 45 °C, R_{air} span was between 288 J/kgK at 0% LP-EGR with 10% RH and 299 J/kgK at 10% LP-EGR with 70% RH. The gas density reduction at high specific humidity was caused by the water content increase in the air, leading to a lower molecular weight that increased the gas constant and thus reduced the gas density, according to the ideal gas state equation.

The gas constant effect is analysed in Fig. 5. The main-external axes represent the engine operation point, with engine speed on the x-axis and engine load on the y-axis. The gas constant and the fresh air mass flow are expressed in percentage variation at the internal x-axis and the y-axis, respectively, for every marker of the principal axes. The colours represent the relative humidity and the different symbols account for the LP-EGR rate. Fig. 5 shows how the fresh air mass flow decreases linearly with the gas constant increase due to humidity. The reduction slope slightly increased with the engine speed.

Focusing on the different symbols (LP-EGR rate) for a particular colour (humidity level), Fig. 5 shows how the fresh air mass flow decreased when the LP-EGR rate increased. The volumetric efficiency was also reduced since the mass flow decrease was higher than the gas constant increase. The charge air heats up during the intake stroke due to heat transfer from the cylinder walls, increasing temperature, and specific volume. The growth of specific volume changed in magnitude for a constant temperature increment due to the different gas constants at each point. Accordingly, the specific volume increment was higher as the specific humidity increased. Hence, the amount of charge air mass that entered the cylinder was affected and, thus, the engine's volumetric efficiency.

In summary, the increase in gas constant due to higher humidity had two penalty effects. On the one hand, it reduced the intake charge density for the same pressure, temperature, and displaced volume. On the other hand, it also reduced the volumetric efficiency by increasing the dilatation capability of in-cylinder gas during the engine intake stroke.

The engine's volumetric efficiency and air density reduction were not the only phenomena that affected the amount of available O_2 in the combustion process. As the air transported a higher amount of water, there was a substitution of O_2 by water, further reducing the available O_2 because of its lower concentration in the charge air mass flow. This phenomenon is observed in.

Fig. 6 confronts the percentage of air mass flow decrease due to EGR rate and specific humidity and the percentage of O_2 mass flow reduction. A higher in O_2 than air mass flow occurred at each point due to the O_2 dilution in EGR and/or increased water content. For example, focusing on the engine point of 3000 rpm and 12 bar of BMEP (top right graph), Fig. 6 shows how the fresh air mass flow was reduced by ~7% at 70% RH and 0% LP-EGR rate (brown square). However, O_2 mass flow was

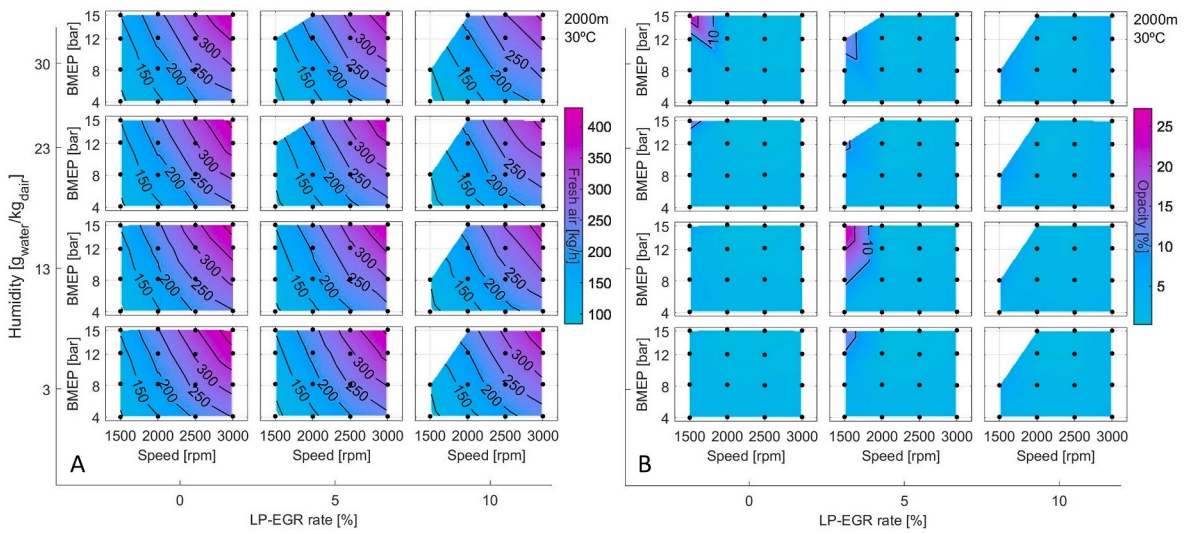

Fig. 2. Effect of ambient humidity: (A) fresh air; (B) opacity. Emulated atmospheric conditions: 2000 m above sea level and 30 °C in ambient temperature.

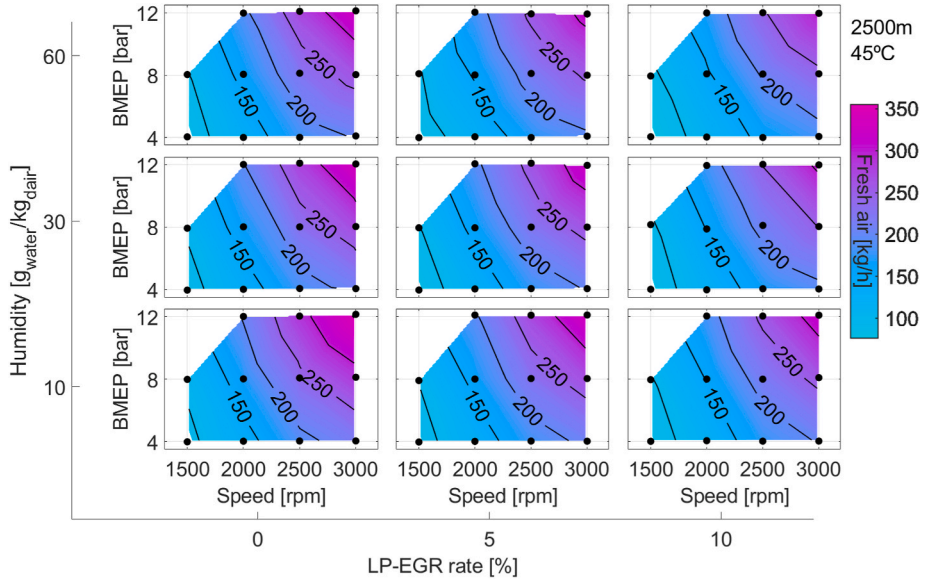

Fig. 3. Effect of water injection: Fresh air mass flow. Emulated atmospheric conditions: 2500 m above sea level and 45 °C in ambient temperature.

decreased by more than 10% in the same operating conditions.

3.2. Impact of humidity on BSFC

The O_2 reduction as the humidity increased due to the lower density and volumetric efficiency (lower fresh air mass flow) and higher water content in the fresh air has been shown in Fig. 4A, which represents the O_2 molar fraction in the exhaust gases. This is a relevant but indirect measurement since the fuel consumption also changed with the specific humidity to reach the target engine BMEP. The variation of the fuel consumption, added to the decrease of the O_2 intake mass flow, led to the enrichment of the combustion process, which decreased the O_2-to-fuel ratio during the combustion. Fig. 7 shows that the O_2-to-fuel ratio decreased as the specific humidity and LP-EGR rate increased. Consequently, a considerable increase in the moisture of the fresh air reduces the engine efficiency due to the lower O_2-to-fuel ratio obtained.

The BSFC increased clearly within the Earth humidity range (Fig. 8A) and for forced humidity levels (Fig. 8B). As the water content of the intake air (for the same pressure and temperature) increased, the O_2-to-fuel ratio also did. The effect is consistently shown in Fig. 8 independently of the EGR rate, the altitude tested, the intake temperature, and the engine operating point (BMEP & speed). If one compares Fig. 8A with Fig. 8B, the effect of altitude and temperature in the BSFC for points with the same BMEP, specific humidity, speed, and EGR rate can be observed, finding higher BSFC in Fig. 8B because of the higher altitude and ambient temperature. The differences are more important at low BMEP and high EGR rates.

3.3. Impact of humidity on NOx

Concerning pollutant emissions, Fig. 9A shows how the engine-out NO_x emissions decreased when humidity increased (from bottom to upper charts). As expected, this reduction was also observed as the EGR rate increased (from left to right charts). The engine-out NO_x emissions were reduced by 50% when the specific humidity rose from 3 to 30 g_{water}/kg_{air}. As a result, when one combines high humidity and EGR rate (top-right chart), the engine-out NOx emission is significantly reduced compared to the dry case and closed LP-EGR valve (bottom-left chart).

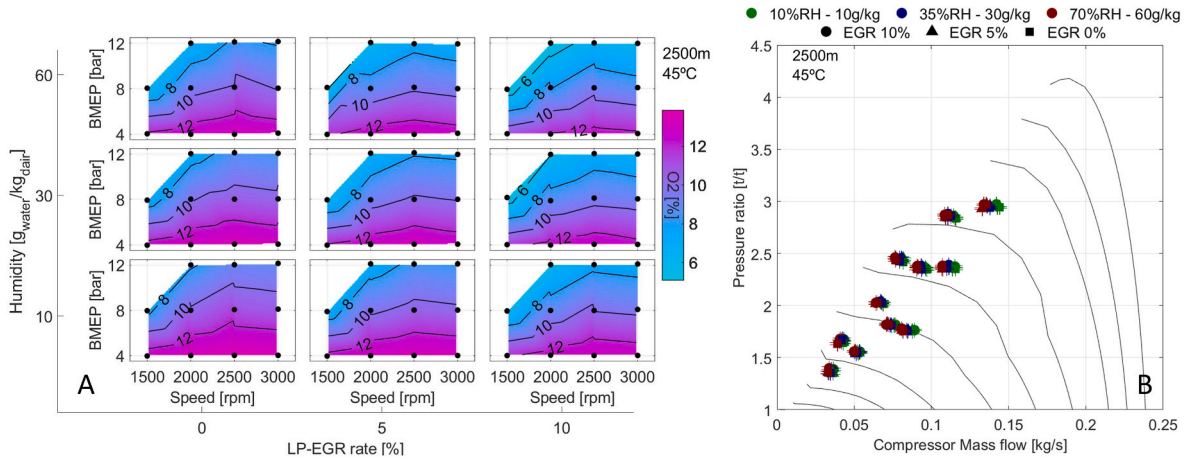

Fig. 4. Effect of water injection: (A) O_2 in the exhaust; (B) compressor map. Emulated atmospheric conditions: 2500 m above sea level and 45 °C in ambient temperature.

$$R_{air} = R_{N_2} Y_{N_2} + R_{O_2} Y_{O_2} + R_{CO_2} Y_{CO_2} + R_{H_2O} Y_{H_2O} + R_{Ar} Y_{Ar} \quad (2)$$

$$\eta_V = \frac{\dot{m}}{\frac{p}{T \bullet R_{air}} V_D \frac{n}{2}} \quad (3)$$

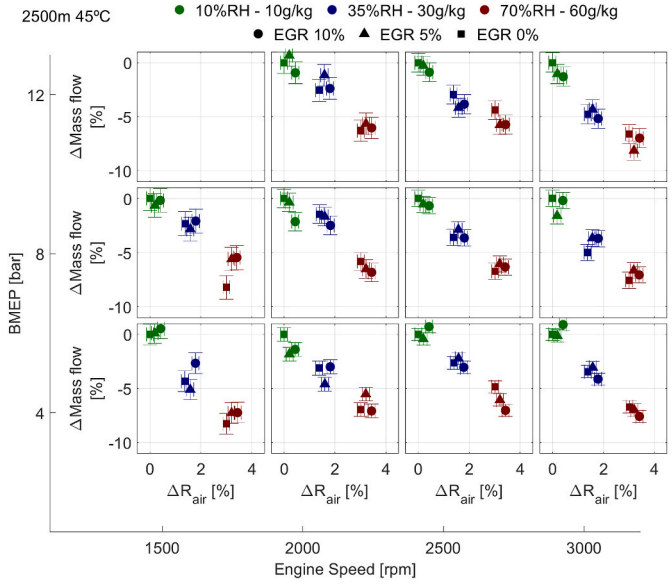

Fig. 5. Effect of the gas constant change over the fresh air mass flow in relative values. Emulated atmospheric conditions: 2500 m above sea level and 45 °C in ambient temperature.

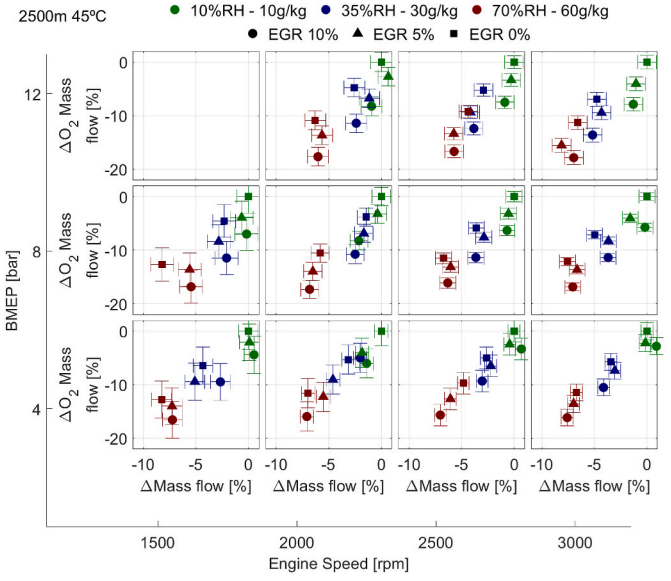

Fig. 6. O_2 reduction due to the substitution for water vapour. Emulated atmospheric conditions: 2500 m above sea level and 45 °C in ambient temperature.

These results highlight the interest in NO_x emission control based on ambient humidity, thus affecting the calibration of the EGR strategy, provided that an ambient humidity sensor is included in the engine intake. In that case, it would be possible to meet the objective of engine-out NOx emissions with lower EGR rates. It would reduce fuel consumption, avoiding EGR impact just dealing with the penalty caused by the ambient specific humidity increase. Fig. 8. Effect of specific humidity and LP-EGR rate on BSFC at A) 2000 m and 30 °C in ambient temperature and B) 2500 m and 45 °C in ambient temperature.

Complementary, Fig. 9B explores the previous results regarding the positive impact of high water content in the fresh air to reduce engine-out NOx emissions emulating water addition to the air as a technique beyond the ambient humidity levels. Considering these results, the injection of water in the intake line of a compression-ignition engine provided the same potential in NO_x control as the well-established EGR strategies. Fig. 9B shows that increasing humidity from 10 g_{water}/kg_{air} to 60 g_{water}/kg_{air} was more efficient for NOx reduction than EGR from 0% to 10%. In fact, the combination of 60 g_{water}/kg_{air} and 10% EGR reduced the engine-out NOx emissions more than five times. These results underline the potential of water injection to control NO_x, especially at high altitudes (like 2500 m), where the possibility of using high EGR rates is limited by the thermomechanical limits of the turbochargers [16].

Fig. 10A shows the trade-off between the NO_x emissions and the BSFC. For all tested points, the different EGR rates and specific humidities of the fresh air collapsed in the same trend. It can be concluded that the trade-off between engine-out NOx emissions and BSFC was not affected by using EGR or specific humidity to control NOx emissions

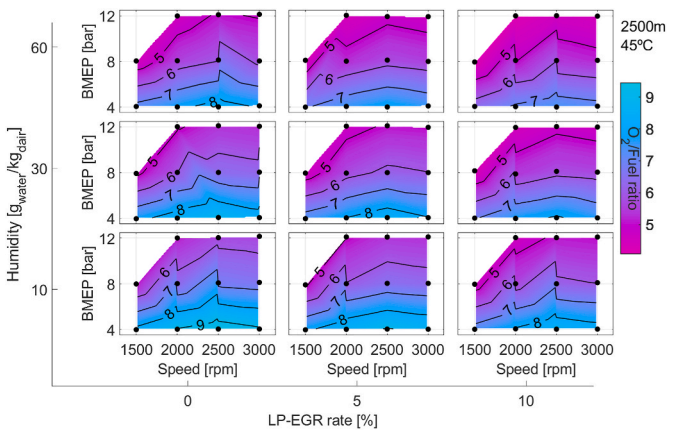

Fig. 7. Effect of specific humidity and LP-EGR rate on O_2-to-fuel ratio at 2500 m and 45 °C in ambient temperature.

with the same impact from the BSFC point of view. It was especially evident as the engine load and speed increased (12 bar and 3000 rpm). Therefore, if ambient conditions impose high specific humidity, the engine control should reduce the EGR rate to take advantage of the potential to reduce NOx emissions, avoiding excessive fuel economy penalty. In parallel, forced water injection may be explored when EGR is not advisable or possible because of the negative impact on the turbocharger operation.

As discussed in Fig. 2B, the water content of the charge air had a relevant impact on exhaust gas opacity. In this regard, Fig. 10B compares the trade-off between engine-out NOx emissions and opacity for each operating point as a function of the EGR rate and the specific humidity. At low engine speeds, no significant difference between controlling NO_x with water injection or EGR rate was noticed in the trade-off between these variables. The NOx emission became lower as the specific humidity increased and was more sensitive to water than to LP-EGR at the studied rates. Again, the low sensitivity of engine-out NOx emissions to EGR rate is critical for optimal NOx emission control at high altitudes since the maximum LP-EGR rates are limited by engine and turbocharger thermo-mechanical limits [16]. Moreover, the trade-off between NO_x and opacity improved at high speeds and even more at high loads, i.e. 3000 rpm and 12 bar of BMEP (top right graph), in the case of the water content increase. Fig. 10B shows how opacity is always lower in the case of higher specific humidity for a given NOx emission amount.

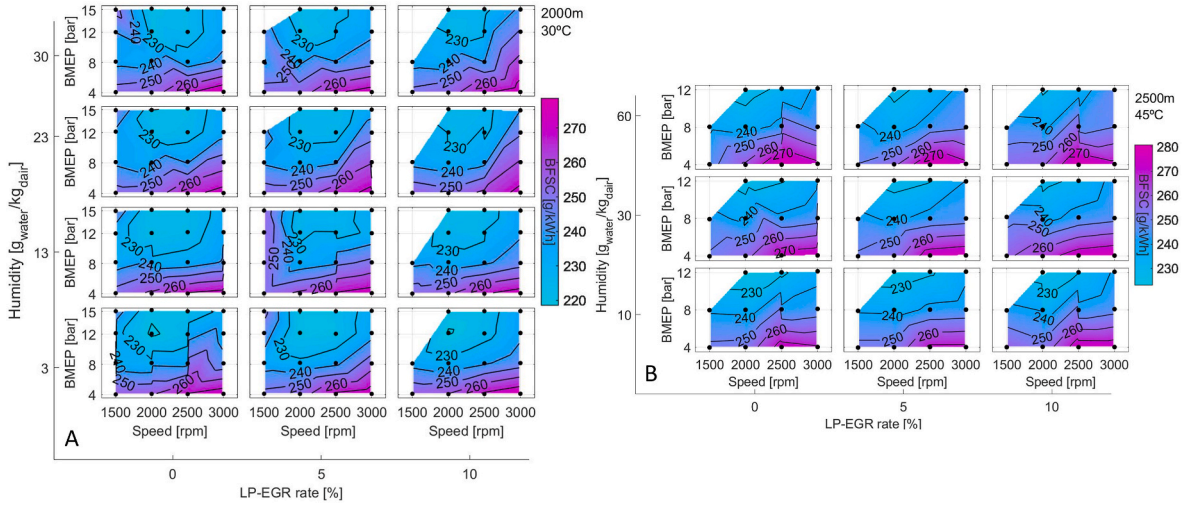

Fig. 8. Effect of specific humidity and LP-EGR rate on BSFC at A) 2000 m and 30 °C in ambient temperature and B) 2500 m and 45 °C in ambient temperature.

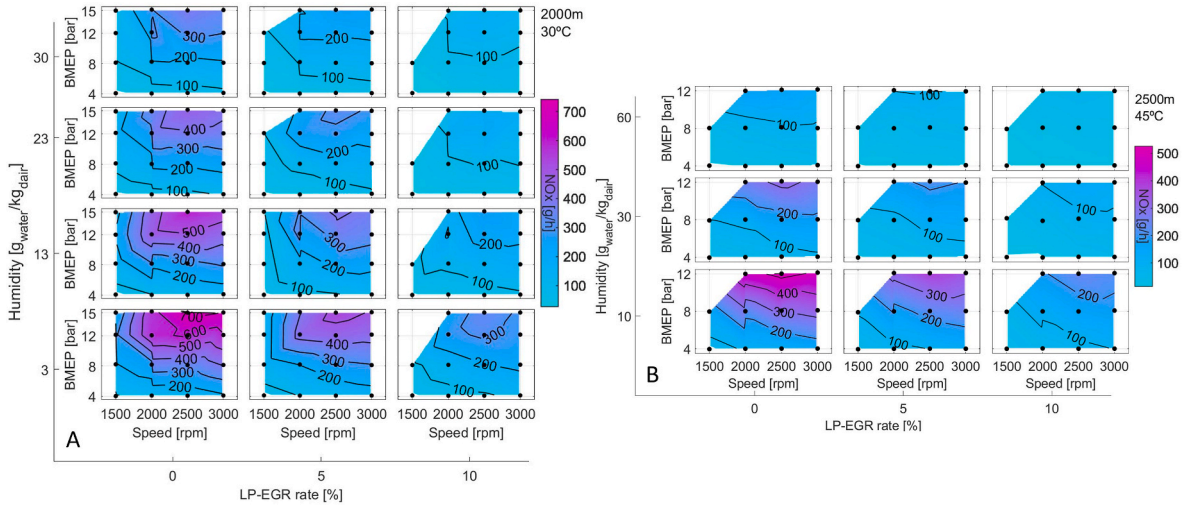

Fig. 9. Effect of specific humidity and LP-EGR rate on engine-out NOx emissions at A) 2000 m and 30 °C in ambient temperature and B) 2500 m and 45 °C in ambient temperature.

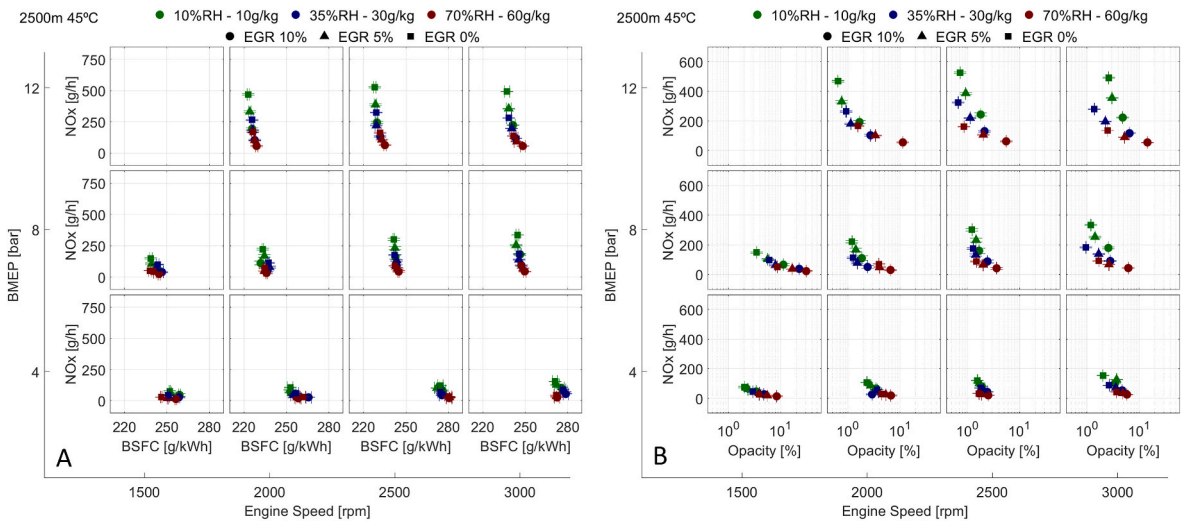

Fig. 10. Effect of specific humidity and LP-EGR rate at 2500 m above sea level and 45 °C in ambient temperature on A) NOx-BSFC trade-off and B) NOx-opacity trade-off.

To understand the change in the trade-off between NOx and opacity caused by the variation of the specific humidity, the combustion temperature and heat release law corresponding to 3000 rpm and 12 bar of BMEP were analysed in more detail. Concerning NO_x emissions, Fig. 11A shows the in-cylinder gas temperature as a function of the crankshaft angle for each EGR rate. The results evidenced that the engine-out NO_x emission reduction did not correlate with the maximum gas temperature decrease. The maximum gas temperature increased as the specific humidity did, as it reduced the O_2-to-fuel ratio, as shown in Fig. 7. Therefore, the NO_x emissions reduction cause is the lower O_2 availability. The difference in the in-cylinder temperature along the late combustion could also explain the improvement found in the NO_x to opacity trade-off (Fig. 10B) when the NO_x is controlled by increasing the humidity of the fresh air instead of by EGR rate. During the diffusive combustion of the post-injection (around crank angle 40° aTDC), the PM produced during the main combustion phase is oxidised [32,33]. Therefore, similarly to what happens with water injection, a higher temperature along this phase favours the oxidation and reduces the engine-out PM. In parallel, no significant temperature difference was found among EGR rate cases during the combustion of the post-injected fuel, especially between 5% and 10%. It evidenced the lower impact of the EGR on the NO_x to opacity ratio found experimentally.

The results obtained regarding the rate of heat release (RoHR) through the combustion are shown in Fig. 11B. An increasing delay in the heat release rate with the increase of specific humidity was found during the pilot injection combustion, around −10° aTDC (see zoomed red boxes in Fig. 11B). Next, the process remained delayed during the main combustion stage, starting around 0° aTDC, although its magnitude was much smaller than that observed during the pilot combustion. Moreover, the heat release rate peak decreased as the humidity increased. These two phenomena, i.e., the combustion delay and the lower maximum heat released rate, caused the engine efficiency reduction with the increased humidity (Fig. 10A). Such an effect produced a snowball process where the efficiency reduction led to increase the injected fuel mass to maintain the target torque. In turn, decreased further the O_2-to-fuel ratio, converging to those shown in Fig. 7.

The combustion timing effects are finally summarised in Fig. 12, where the combustion completeness angles (from 10% to 90%) are represented. In cases with 0% and 5% EGR rates, the specific humidity increase from 10 g_{water}/kg_{dry_air} to 30 g_{water}/kg_{dry_air} showed a slight increase in the combustion speed during the initial combustion stage (CA10), but later the global trend was followed. Further increment of the specific humidity to 60 g_{water}/kg_{dry_air} delayed the combustion from CA10 to CA90, ranging from 0.5° at CA10 up to 3.7° at CA90 with 10%

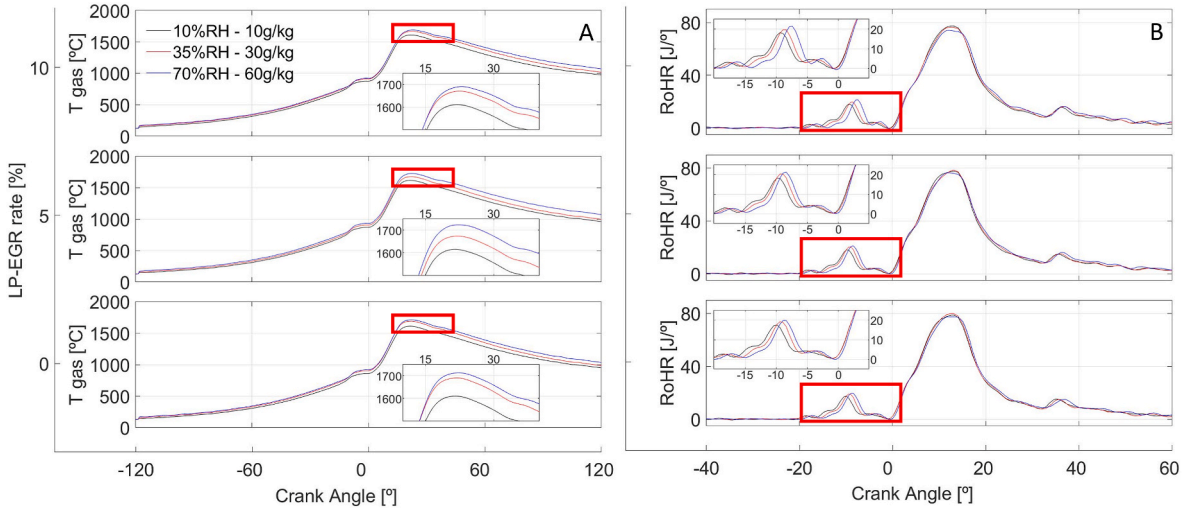

Fig. 11. Effect of specific humidity and LP-EGR rate on A) the in-cylinder temperature and B) the rate of heat release.

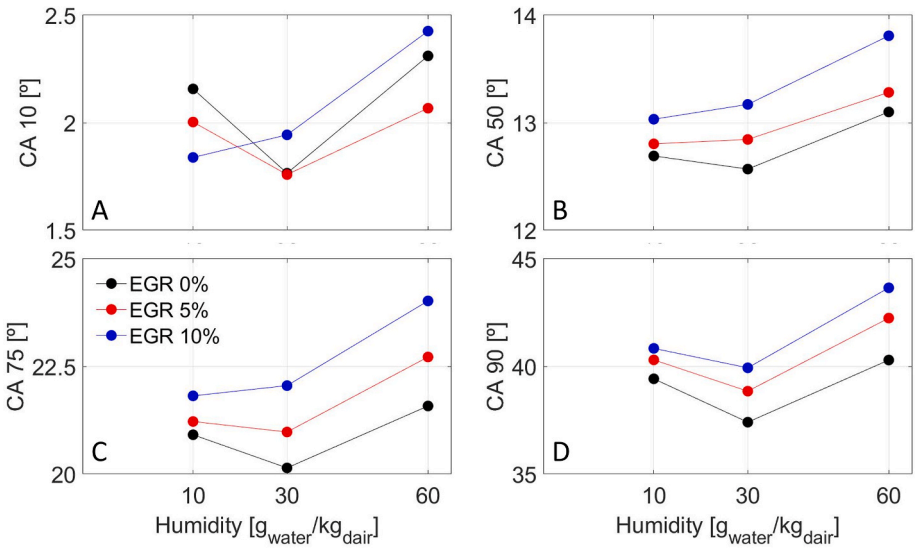

Fig. 12. Effect of specific humidity and LP-EGR rate on the combustion completeness: A) CA10, B) CA50, C) CA75, and D) CA90.

in LR-EGR rate.

3.4. Impact of humidity on other regulated emissions

Lastly, the engine-out emission of CO_2 and the rest of the regulated pollutant emissions are plotted in Fig. 13 for a change in specific

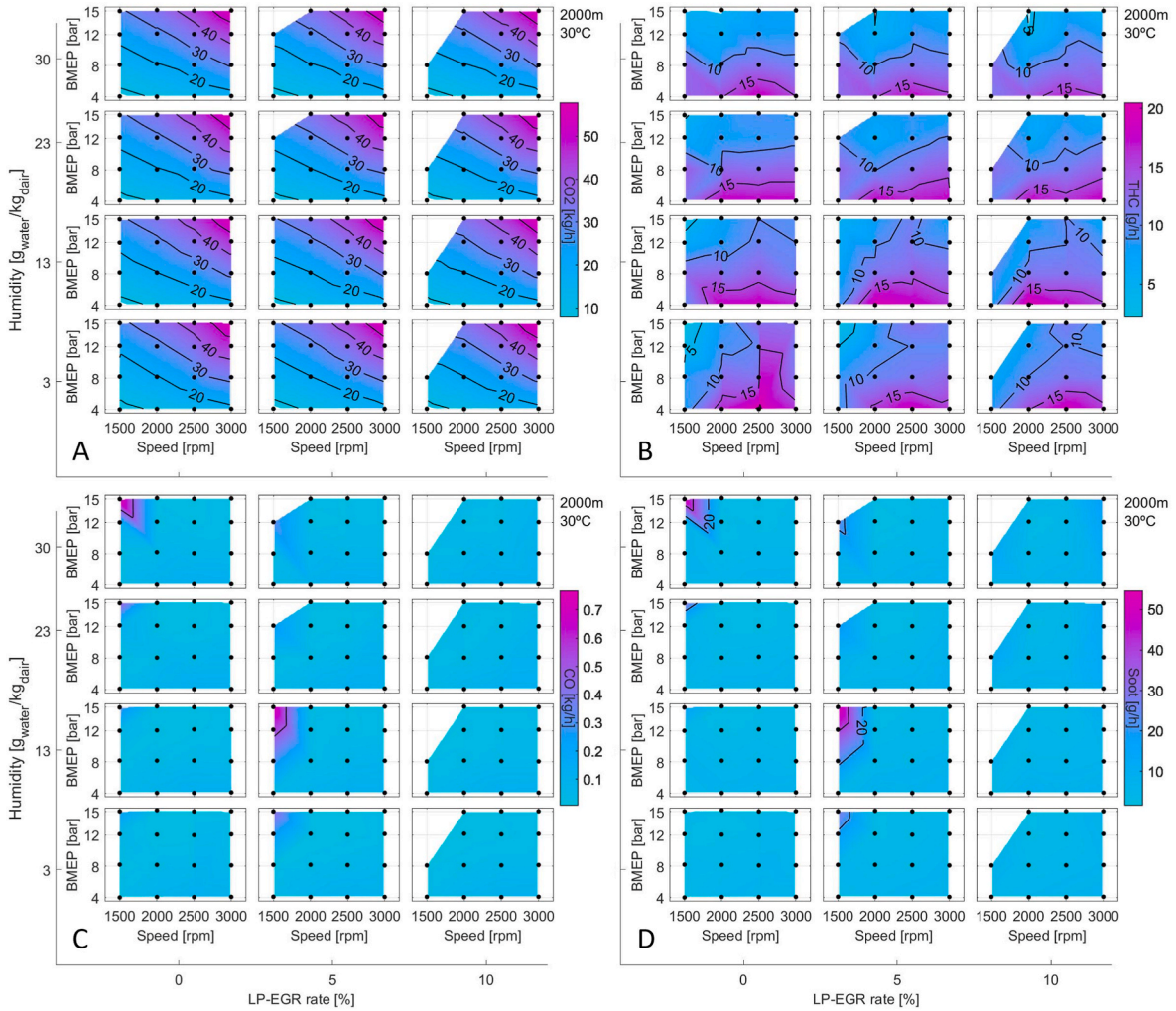

Fig. 13. Effect of ambient humidity: (A) CO_2; (B) THC; (C) CO; (D) Soot. Atmospheric conditions: 2000 m above sea level, 30 °C.

humidity between realistic atmospheric levels at 30 °C and 2000 m. The emitted CO_2 mass flow is represented in Fig. 13A. It shows the expected trend according to the discussion on BSFC from Fig. 8A. CO and soot emissions are plotted in Fig. 13C and D. The pollutants can be analysed together since their trends obey the same cause. In both charts, the emission increased as the ambient humidity did. This increment was caused by the higher content of inert gas (water vapour) in the charge air, which led to lower O_2 availability and to incomplete combustion that converged to a higher amount of these two pollutants. Specifically, the THC emissions, plotted in Fig. 13B), showed a slight decrease when the specific humidity increased. The THC slightly decreased from the bottom row to the medium row of Fig. 13B and then dropped sharply when moving to the top row of Fig. 13B.

Finally, Fig. 14A and Fig. 14B show the CO and THC emission corresponding to the engine operation at 2500 m and 45 °C of ambient conditions and increasing the specific humidity of the fresh air up to 60 g_{water}/kg_{dry_air}. Since these two pollutants are related to the combustion quality, the higher the combustion efficiency, the lower these two pollutant emissions are. The results confirmed that both emissions increased at higher altitude and temperature as the specific humidity did. At the same time, the impact of the LP-EGR rate was mostly negligible for these pollutant species. Still, there was an inflection point in the charge air water content between 30 and 60 g_{water}/kg_{dry_air} since the THC emission increased sharply. The reasons for these results are again found in the decreasing O_2-to-fuel ratio previously depicted in Fig. 7 and the slower combustion (Fig. 12) resulting from the specific humidity increase.

4. Conclusions

Several conclusions related to the effect of charge air humidity on turbocharged compression-ignition engine performance and pollutant emissions operating at warm & hot altitudes can be stated:

- The high water content in the charge air flow causes a reduction in the engine efficiency due to the induced slowing down of the combustion process. The beginnings of the premixed and main combustion phases were delayed by around 2.5 CAD and 1 CAD, respectively, and the heat released during the main combustion was reduced.
- The increase in specific humidity of air affects the amount of O_2 available during the combustion in three ways. Firstly, it causes a decrease in the charge air density, which reduces up to 7% of the intake mass flow for a given intake manifold pressure and temperature within the tested ranges. Secondly, the composition of the charge air flow changes when the humidity increases, reducing the amount of dry air by replacing it with water vapour. Finally, the higher water content in the charge air flow reduces the engine's volumetric efficiency. The latter happens due to the change in composition, which directly affects the gas constant and the specific volume of the mixture. As the water content increases, the differences in gas constant increase the expansion rate inside the cylinder for a given heat flux during the intake stroke, thus causing the volumetric efficiency reduction.
- The air humidity was also found to affect all the pollutant emissions. The engine-out CO and PM emissions increased as the humidity did due to the reduction of the O_2-to-fuel ratio, similar to the EGR rate increase impact. The THC emissions were also penalised in line with the combustion delay. Contrarily, the NO_x emissions decreased significantly (up to 300% with respect to the dry case) when the charge air humidity increased. The results evidence a high potential for NO_x emission control at high loads than more common strategies like LP-EGR, especially in altitude driving conditions where the turbocharger operation limits the EGR use. In these cases, it is possible to achieve the objective of engine-out NOx emissions with lower EGR rates and fuel consumption avoiding any trade-off between engine performance and NOx emissions. The engine-out NO_x emissions decreased according to the O_2 reduction attributed to the higher equivalence ratio and the substitution of O_2 by water vapour instead of a drop in the maximum in-cylinder temperature.
- Despite the existing trade-off between engine-out NOx and PM emissions, the control of NO_x through the specific humidity of the charge air flow provides better results in PM emissions than the traditional control based on LP-EGR. The increased specific humidity reduced the engine-out opacity up to 250% with respect to LR-EGR technique for the same in engine-out NOx emission. The reason lies in the combustion enhancement during the late combustion phase because of the higher unburned fuel available when the post-injection occurs, which is caused by the combustion delay and the increase in injected fuel mass. Both aspects increase the temperature during the late combustion phase, which favours the PM oxidation and results in the observed engine-out opacity reduction.

Credit author statement

José Ramón Serrano: Funding acquisition, Project administration, Supervision, Methodology, Writing – original draft, Writing – review & editing.Jaime Martín: Conceptualization, Formal analysis, Writing – original draft, Writing – review & editing.Pedro Piqueras: Funding acquisition, Conceptualization, Formal analysis, Writing – original draft, Writing – review & editing.Roberto Tabet: Investigation, Visualization, Writing – original draft, Writing – review & editing.Javier Gómez: Methodology, Writing – review & editing

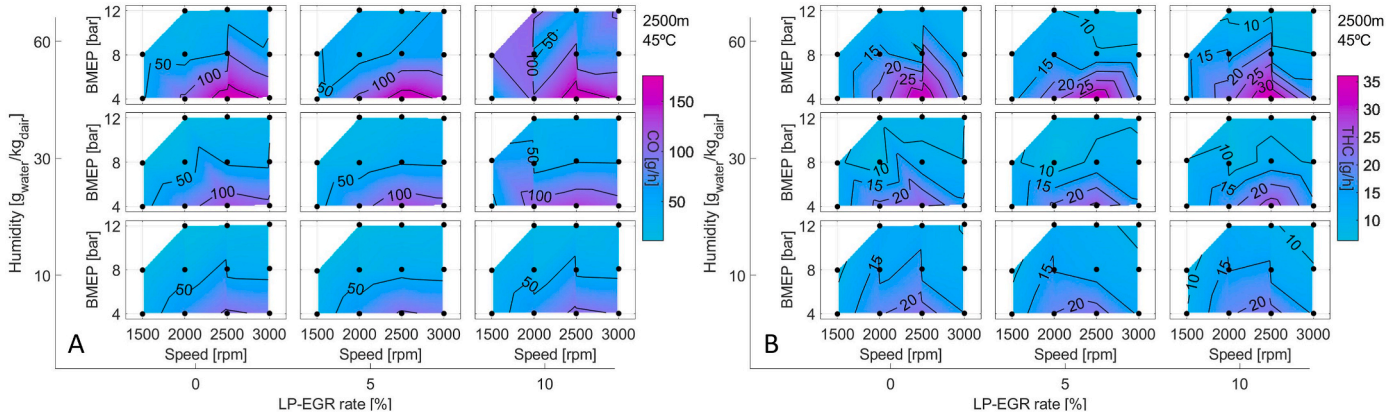

Fig. 14. Effect of water injection: (A) CO emissions; (B) THC emissions. Emulated atmospheric conditions: 2500 m above sea level and 45 °C in ambient temperature.

Declaration of competing interest

The authors declare that they have no known competing financial interests or personal relationships that could have appeared to influence the work reported in this paper.

Data availability

Data will be made available on request.

Acknowledgements

This research has been supported by Grant PID2020-114289RB-I00 funded by the Spanish Ministerio de Ciencia e Innovación – Agencia Estatal de Investigación (MCIN/AEI/10.13039/501100011033) . The PhD candidate Roberto Tabet has been funded by Universitat Politècnica de València through grant PAID-01-18.

References

[1] Boger T, Rose D, He S, Joshi A. Developments for future EU7 regulations and the path to zero impact emissions – a catalyst substrate and filter supplier's perspective. Transport Eng 2022;10:100129.
[2] Incropera FP, DeWitt DP. Fundamentals of heat and mass transfer. fourth ed. Pearson Educación; 1999.
[3] Block Novelo DA, Iggie U, Prakash V, Szymański A. Experimental investigation of gas turbine compressor water injection for NOx emission reductions. Energy 2019; 176(1):235–48.
[4] Li A, Zheng Z, Song Y. A simulation study of water injection position and pressure on the knock, combustion, and emissions of a direct injection gasoline engine. ACS Omega 2021;6(28):18033–53.
[5] Loaiza JL, Vaqueiro J. Model of water injection process during closed phase of spark ignition engine. Energy 2019;174(1):1121–32.
[6] Domingos D, de Castro F, Santos G, Brunocilla MF, de Ferreira PC, Duarte N, Teixeira AC, Rodrigues FA, Coelho JG. Study of the water injection control parameters on combustion performance of a spark-ignition engine. Energy 2021; 217:119346.
[7] Chen Z, Cai Y, Xu G, Duan H, Jia M. Exploring the potential of water injection (WI) in a high-load diesel engine under different fuel injection strategies. Energy 2022; 243:123074.
[8] Ma X, Zhang F, Han K, Zhu Z, Liu Y. Effects of intake manifold water injection on combustion and emissions of diesel engine. Energy Proc 2014;61:777–81.
[9] Hountalas DT, Mavropoulos GC, Zannis TC, Mamalis SD. Use of water emulsion and intake water injection as NOx reduction techniques for heavy duty Diesel engines. SAE Technical Paper 2006;(1):1414.
[10] Tauzia X, Maiboom A, Shah SR. Experimental study of inlet manifold water injection on combustion and emissions of an automotive direct injection Diesel engine. Energy 2010;35(9):3628–39.
[11] Kettner M, Dechent S, Hofmann M, Huber E, Arruga H, Mamat R, et al. Investigating the influence of water injection on the emissions of a diesel engine. J Mech Eng Sci 2016;10(1):1863–81.
[12] Subramanian KA. A comparison of water-diesel emulsion and timed injection of water into the intake manifold of a diesel engine for simultaneous control of NO and smoke emissions. Energy Convers Manag 2011;52(2):849–57.
[13] Ayhan V, Mert Ece Y. New application to reduce NOx emission of diesel engines: electronically controlled direct water injection at compression stroke. Appl Energy 2020;260:114328.
[14] Chen Z, Cai Y, Xu G, Duan H, Jia M. Exploring the potential of water injection (WI) in a high-load diesel engine under different fuel injection strategies. Energy 2022; 243:123074.
[15] Zhang H, Shi L, Deng K, Liu S, Yang Z. Experiment investigation on the performance and regulation rule of two-stage turbocharged diesel engine for various altitudes operation. Energy 2020;192:116653.
[16] Bermúdez V, Serrano JR, Piqueras P, Diesel B. Fuel consumption and aftertreatment thermal management synergy in compression ignition engines at variable altitude and ambient temperature. Int J Engine Res 2021. https://doi.org/10.1177/14680874211035015. published online.
[17] Liu J, Wang B, Meng Z, Liu Z. An examination of performance deterioration indicators of diesel engine on the plateau. Energy 2023;262:125587.
[18] Zhang C, Li Y, Liu Z, Liu J. An investigation of the effect of plateau environment on the soot generation and oxidation in diesel engines. Energy 2022;253:124086.
[19] Chen S, Liu C, Wu Z, Yu Q. Effects of co-current airflow on water atomization in a curved diffuser. Energy Explor Exploit 2021;39(2):657–68.
[20] Armstrong International Inc. Conditioned steam humidifiers. 2020. Accessed: Jan. 19, 2022. Available: https://haarla.fi/wp-content/uploads/2021/06/Conditioned-Steam-Humidifiers-598-20171101.pdf.
[21] Serrano JR, Gil A, Quintero P, Tabet R, Gómez J. Design of a bubble reactor for altitude simulators used to humidify a combustion air stream by means of CFD multi-phase models. Appl Sci 2021;11(1):1–15.
[22] Serrano JR, Piqueras P, Abbad A, Tabet R, Bender S, Gómez J. Impact on reduction of pollutant emissions from passenger cars when replacing Euro 4 with euro 6d diesel engines considering the altitude influence. Energies 2019;12(7).
[23] Desantes JM, Galindo J, Payri F, Piqueras P, and Serrano JR. "Device for conditioning the atmosphere in tests of alternative internal combustion engines, method and use of said device." WO 2016/116642 A1.
[24] Desantes JM, Benajes J, Serrano JR, Bermúdez V, Piqueras P, Gómez J, et al. Device, method and use for conditioning intake air for testing internal combustion engines. 2019. WO.
[25] Broatch A, Bermúdez V, Serrano JR, Tabet R, Gómez J, Bender S. Analysis of passenger car turbocharged diesel engines performance when tested at altitude and of the altitude simulator device used. J Eng Gas Turbines Power 2019;141(8).
[26] Serrano JR, Piqueras P, Sanchis EJ, Diesel B. Analysis of the driving altitude and ambient temperature impact on the conversion efficiency of oxidation catalysts. Appl Sci 2021;11(3):1283.
[27] Piqueras P, Burke R, Sanchis EJ, Diesel B. Fuel efficiency optimisation based on boosting control of the particulate filter active regeneration at high driving altitude. Fuel 2022;319:123734.
[28] Roberts P, Mason A, Headley A, Bates L, Whelan S, Tabata K. RDE plus - a road to rig development methodology for whole vehicle RDE compliance: road to engine perspective. 2021. *SAE Technical Paper* 2021-01-1223.
[29] Kuttippurath J, Murasingh S, Stott PA, Balan B, Jha MK, Kumar P, et al. Observed rainfall changes in the past century (1901–2019) over the wettest place on Earth. Environ Res Lett 2021;16(2):024018.
[30] Olmeda P, Tiseira A, Dolz V. García-Cuevas LM "Uncertainties in power computations in turbocharger test bench" *Measurement* 2015;59:363–71.
[31] de Nicolao G, Scattolini R, Siviero C. Modelling the volumetric efficiency of IC engines: parametric, non-parametric and neural techniques. Control Eng Pract 1996;4(10):1405–15.
[32] Lautenberger CW, de Ris JL, Dembsey NA, Barnett JR, Baum HR. A simplified model for soot formation and oxidation in CFD simulation of non-premixed hydrocarbon flames. Fire Saf J 2005;40(2):141–76.
[33] Fach C, Rödel N, Schorr J, Krüger C, Dreizler A, Böhm B. Multi-parameter imaging of in-cylinder processes during transient engine operation for the investigation of soot formation. Int J Engine Res 2021. https://doi.org/10.1177/14680874211019976. published on-line.